Magnetic signature of European margin sediments: Provenance of ice-rafted debris and the climatic response of the British ice sheet during Marine Isotope Stages 2 and 3

Clare Peters,[1] John Walden,[1] and William E. N. Austin[1]

Received 23 May 2007; revised 1 May 2008; accepted 27 May 2008; published 24 July 2008.

[1] Mineral magnetic measurements are used to distinguish ice-rafted debris (IRD) sources and climate cycles spanning Marine Isotope Stage (MIS) 3 and MIS2 in core MD95–2006, from the Barra Fan, NE Atlantic. Distinct magnetic properties are displayed by IRD from the Laurentide ice sheet (LIS) (high susceptibility (χ), low isothermal remanent magnetization (IRM), low coercivity and the Verwey transition), the British ice sheet (BIS) (high χ, high IRM, medium coercivity and suppressed Verwey transition) and the ambient background sediment (low χ and low IRM). A magnetic unmixing model quantifies proportions of the IRD sources during Greenland Stadial (GS) 16 to GS3 (57.3 to 22.6 ka B.P.) spanning Heinrich Event (H) 5 to H2. The magnetic model suggests LIS IRD is only dominant within an interval during GS9, assigned to H4. Prior to H4 low proportions of BIS IRD suggest the BIS was not able to deliver significant amounts of IRD into the marine system. Following H4, proportions of BIS IRD during stadials increase, suggesting growth of the BIS during the latter stages of MIS3, with further expansion of the BIS during MIS2. LIS IRD within H2 is masked by BIS IRD input. Climatically driven anhysteretic remanent magnetizations reflect the short Dansgaard-Oeschger cycles between H5 and H4, while the proportions of hard magnetic minerals reflect the longer-term Bond cycles.

Citation: Peters, C., J. Walden, and W. E. N. Austin (2008), Magnetic signature of European margin sediments: Provenance of ice-rafted debris and the climatic response of the British ice sheet during Marine Isotope Stages 2 and 3, *J. Geophys. Res.*, *113*, F03007, doi:10.1029/2007JF000836.

1. Introduction

[2] Links between variations in atmospheric temperatures, ocean circulation and ice sheet instability are now well established during the last glaciation in the North Atlantic region. However, the mechanisms driving and/or triggering the abrupt climate changes associated with these variations are still to be unequivocally resolved. Correlation of planktonic foraminiferal abundance in North Atlantic deep-sea sediments, reflecting sea surface temperatures, to atmospheric temperature reflected in the $\delta^{18}O$ of Greenland ice cores, was first demonstrated by *Bond et al.* [1993]. Warm interstadial events (Dansgaard-Oeschger (D-O) events) in the ice core records were numbered Greenland Interstadial (GI) 1 to GI24 [*Johnsen et al.*, 1992; *Dansgaard et al.*, 1993] and extended back to Greenland Stadial (GS) 26, the beginning of the last glacial period [*North Greenland Ice Core Project Members*, 2004] at approximately 119 ka B.P. Groups of D-O events showed a longer-term cooling trend culminating in major warming events (Bond cycles) [*Bond et al.*, 1993]. The coldest events of the Bond cycles, embedded within the stadials immediately prior to the major abrupt warming, temporally coincided with enormous discharges of icebergs into the North Atlantic, termed Heinrich events (HEs) by *Broecker et al.* [1992] after *Heinrich* [1988]. Six HEs have commonly been documented between 10 ka B.P. and 60 ka B.P. [*Hemming*, 2004]. The duration of the Bond cycles between the six HEs is not uniform. However, an additional HE was suggested by *Rashid et al.* [2003] between H5 and H6, labeled H5a, and its inclusion suggested more uniform temporal spacing of the Bond cycles between H1 to H6 at ~7 ka.

[3] Detrital dolomitic carbonate is a defining component of Heinrich layer (HL) ice-rafted debris (IRD) and was sourced to the Laurentide ice sheet (LIS) [*Andrews and Tedesco*, 1992; *Bond et al.*, 1993; *Grousset et al.*, 1993; *Hillaire-Marcel et al.*, 1994; *Bond and Lotti*, 1995; *Andrews*, 1998; *Hemming*, 2004]. The detrital dolomitic carbonate layers were traced for more than 3000 km from the Labrador Sea across the North Atlantic to Iberia, decreasing in thickness from west to east [*Bond et al.*, 1992; *Dowdeswell et al.*, 1995]. The main region in which the detrital dolomitic carbonate layers occur was termed the Ruddiman IRD belt (40–55°N) [after *Ruddiman*, 1977; *Dowdeswell et al.*, 1995] (Figure 1). *Robinson et al.* [1995] correlated cores from the Ruddiman belt on the basis of elevated magnetic suscepti-

[1]Environmental Change Research Group, School of Geography and Geosciences, University of St. Andrews, St. Andrews, UK.

0148-0227/08/2007JF000836

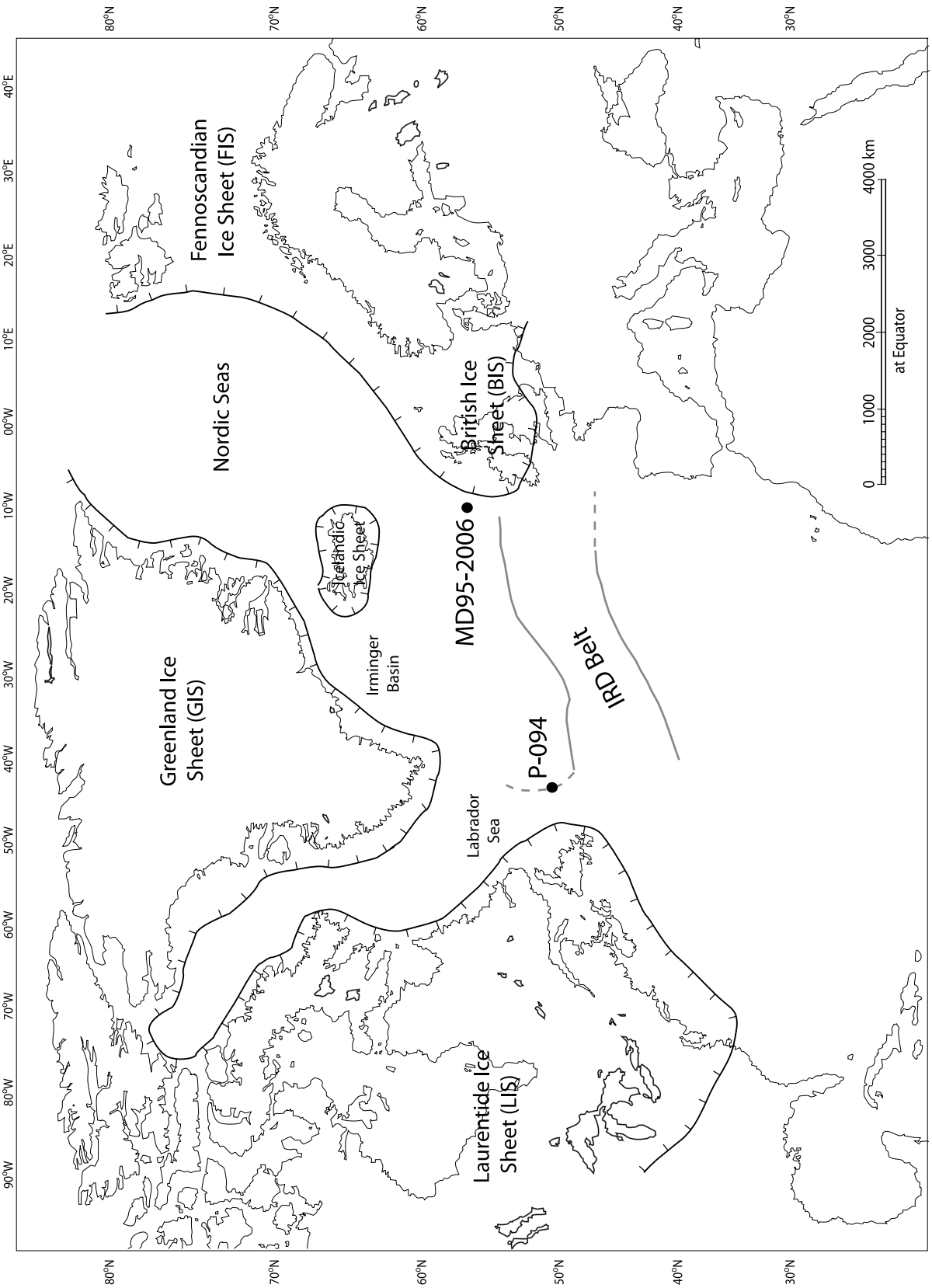
Fennoscandian
Ice Sheet (FIS)
Nordic Seas
British Ice
Sheet (BIS)
MD95-2006
Icelandic
Ice Sheet
Irminger
Basin
Greenland Ice
Sheet (GIS)
IRD Belt
P-094
Labrador
Sea
Laurentide Ice
Sheet (LIS)
0 1000 2000 3000 4000 km
at Equator
80°N
70°N
60°N
50°N
40°N
30°N
90°W
80°W
70°W
60°W
50°W
40°W
30°W
20°W
10°W
00°W
10°E
20°E
30°E
40°E

Figure 1

bilities of HLs and magnetic susceptibility is now routinely measured on board ship after retrieval of cores. Compositional studies of the IRD petrology and mineralogy [*Andrews and Tedesco*, 1992; *Andrews*, 1998] showed that the HLs contained high concentrations of sand-sized limestone and dolomite fragments while these components were virtually absent in the ambient sediment. *Hillaire-Marcel et al.* [1994] reported that the percentage of carbonate grains in the 63–150 μm fraction within H1–4 was approximately 20–30% in core Hu91-045-094 at the western end of the main IRD belt. In addition, potassium-argon (K-Ar) ages showed that the clay minerals within HLs were very much older than those in ambient sediments and the occurrence of large areas of carbonate source rocks of an age consistent with the K-Ar ages, strongly suggested a Canadian provenance for the carbonate fragments within the IRD [e.g., *Bond et al.*, 1992; *Hemming et al.*, 1998; *Hemming*, 2004]. *Hemming* [2004] summarized other data demonstrating the LIS provenance of IRD associated with HLs but also suggested a more systematic analysis is required to fully quantify the variations in carbonate/dolomite concentrations as some HLs show distinct compositional variations (e.g., H3 and H6).

[4] Two causal mechanisms for HEs have been suggested; (1) fluctuations in iceberg discharge from the LIS represented a response to external climatic forcing [e.g., *Bond et al.*, 1997] or (2) internal feedback mechanisms operating within the LIS were responsible for the cyclicity in IRD production, essentially a binge-purge model of growth and surging/collapse [*MacAyeal*, 1993; *Alley and MacAyeal*, 1994; *Alley et al.*, 2005]. Regardless of the forcing mechanism, the discharge of icebergs into the North Atlantic during HEs was an important feedback within the climate system, as the influx of large volumes of cold, fresh water undoubtedly triggered substantial modification (and possibly near total collapse) in the meridional overturning circulation of the North Atlantic [e.g., *Rahmstorf*, 1996].

[5] While evidence clearly suggested that the LIS was the dominant source of IRD within the North Atlantic [*Bond et al.*, 1993], mineralogical and isotopic data [e.g., *Bond et al.*, 1999; *Snoeckx et al.*, 1999; *Grousset et al.*, 2000; *Scourse et al.*, 2000; *Knutz et al.*, 2001; *Zaragosi et al.*, 2001; *Hemming et al.*, 2002] also indicated IRD contributions from the Greenland (GIS), Iceland (IIS), Fennoscandian (FIS) and British (BIS) ice sheets. The temporal relationship between IRD supplied from the LIS and the various European ice sheets is an important element in any attempt to distinguish between the two causal mechanisms for HEs outlined above. Synchroneity of IRD delivery implies a common external forcing mechanism [*Fronval et al.*, 1995]. In contrast, timing differences could indicate either (1) different internal response times to the same climatic stimuli or (2) that internal instability of the LIS triggered HEs (and possibly the periodicity associated with Bond cycles). Under (2), the smaller European ice masses were perhaps responding to the thermohaline circulation (THC) driven D-O cycles but were also influenced by the LIS collapse during HEs via meltwater driven sea level change. Identification of the provenance of IRD forms a key line of evidence in testing these hypotheses.

[6] At present, the available compositional data does not permit this debate to be resolved. There do appear to be timing differences between the deposition of European and Laurentide IRD, with European IRD events arriving at core sites on the European margin prior to LIS IRD input [e.g., *Scourse et al.*, 2000]. However, in core MD95–2006, located on the Barra Fan, IRD input from British sources appeared to demonstrate a D-O pacing [*Knutz et al.*, 2001], while work in the Nordic Seas also suggested that IRD input was influenced by processes other than HEs [e.g., *Fronval et al.*, 1995; *Dowdeswell et al.*, 1999; *Elliot et al.*, 2002]. *Farmer et al.* [2003] demonstrated that for the Nd isotopic fingerprint the distinction between sources may not be as clear as first thought because considerable overlap existed between the European signatures [e.g., *Grousset et al.*, 2000] and those of the southern LIS draining through the Gulf of St Lawrence. This undermines the use of these isotopic data alone to support the idea of a European IRD ''precursor'' [e.g., *Grousset et al.*, 2000] as a triggering mechanism for HEs via LIS response to sea level forcing.

2. Barra Fan and Core MD95–2006

[7] The Barra Fan extends from the Hebridean continental slope to the NE Rockall Trough [*Holmes et al.*, 1998]. It is composed of Neogene sands and Pleistocene glacigenic sediment [*Armishaw et al.*, 1998] and was the major deposition center of the last BIS [*Wilson and Austin*, 2002]. MD95–2006 (57°01.82 N, 10°03.48 W) (Figure 1) is a 3000 cm giant piston core retrieved in 1995 from the northern edge of the Barra Fan at a water depth of 2120 m by the RV *Marion Dufresne* as part of the IMAGES program [*Knutz et al.*, 2001; *Wilson and Austin*, 2002].

[8] On the basis of sedimentary structure, texture, color and carbonate content, five lithological units were identified in the core [*Kroon et al.*, 2000]. Here we focus on units 5 and 4 spanning Marine Isotope Stage (MIS) 3 and MIS2. The two units contain glacimarine mud with discrete sandy turbidites (1400–2150 cm), hemipelagite to muddy contourite (2150–2400 cm) and silty-muddy contourite (2400–3000 cm) [*Kroon et al.*, 2000; *Knutz et al.*, 2001].

[9] On the basis of total lithic counts of grains 250–500 μm, *Knutz et al.* [2001] identified sixteen intervals of raised lithic concentrations, including intervals temporally coeval with H1–4. Following refinement of the age: depth model, *Wilson and Austin* [2002] estimated the age at the bottom of the core to be 53.8 ka B.P. and tentatively assigned the high lithic interval at ~28 m as containing H5. The frequency of lithic peaks was similar to D-O cycles and suggested the BIS contributed to the millennial-scale pattern of iceberg discharges in the NE Atlantic [*Knutz et al.*, 2001]. At 30 ka B.P. (the MIS3-2 transition [*Martinson et al.*, 1987]), *Knutz et al.* [2001]

Figure 1. Map of the North Atlantic indicating the location of core MD95–2006, studied here, and also P-094, referred to in the text. Also including the Ruddiman IRD belt (based on the 200 mg cm^{-2} ka^{-1} contour lines of ice-rafted sand during the upper part of MIS3 from *Ruddiman* [1977]) and an indication of the ice sheets surrounding the North Atlantic during the maximum of the last glacial period.

observed an abrupt increase in basaltic IRD. They attributed the increase to glaciers carrying eroded material from the Tertiary formations of NW Britain reaching the shelf edge. *Wilson and Austin* [2002] also noted a marked transition in their proxy data at 30 ka B.P. Reflectance, lightness and calcium carbonate percentages demonstrated clear D-O pacing prior to 30 ka B.P. After 30 ka B.P. higher-frequency variations occurred, which did not appear to follow the δ^{18}O Greenland ice core records. *Knutz et al.* [2001], *Wilson and Austin* [2002] and *Wilson et al.* [2002] attributed the increased sediment delivery at 30 ka B.P. to the expansion of the BIS to the outer continental shelf edge in climatic response to the global cooling at the MIS3-2 transition.

[10] The North Atlantic Ash Zone II (NAAZII) tephra was discovered in the Greenland ice cores GRIP and GISP2 [*Grönvold et al.*, 1995; *Zielinski et al.*, 1997], with an age estimate of 53,260 (±2660) years B.P. [*Bender et al.*, 1994; *Meese et al.*, 1994]. The stratigraphy of MD95–2006 was anchored at a depth of 2817 cm to the stratigraphy of the Greenland ice cores by the presence of the NAAZII tephra [*Austin et al.*, 2004]. Compilation of *Neogloboquadrina pachyderma* (sinistral) (*Np*(s)) data [*Austin et al.*, 2004; *Dickson*, 2004; *Leigh*, 2006] in conjunction with the NAAZII tie point defines the interstadial/stadial climatic boundaries of the D-O cycles (Figure 2c). In the modern ocean, the *Np*(s) percentages associated with the location of the polar front are clearly defined [*Pflaumann et al.*, 2003]. The age-depth model for MD95–2006 was constructed from a synchronization of the stadial-interstadial transition depths to the corresponding ages (ice core years before 1990) from the ice core δ^{18}O GRIP ss09 sea record [*Johnsen et al.*, 2001].

[11] *Knutz et al.* [2001] showed that detrital carbonate was not a significant IRD component in MD95–2006, with the exception of one layer (at ~2500 cm depth), which has a high concentration of dolomitic carbonate grains. They attributed the dolomitic carbonate to either glacially weathered material of Irish origin or from the LIS. Further research on this layer by *Leigh* [2006] showed a dolomitic carbonate component (>150 μm) of greater than 20% at a depth of ~2483 cm, with radiogenic isotopic values consistent with LIS-sourced material and the layer was therefore assigned to H4.

[12] The lower half of MD95–2006, spanning MIS3 (a period of reduced global ice volume) and MIS2 (a period of increased global ice volume) is, therefore, well constrained chronologically, contains evidence for the presence of both LIS and BIS sourced IRD and, from the *Np*(s) data, shows a clear association with Greenland ice core climatic records containing evidence of D-O cycles. *Walden et al.* [2007] have demonstrated the clear potential for environmental magnetic analysis to assist in IRD provenance studies within core OMEX-2K off SW Britain. The characteristics of MD95–2006 outlined above suggest that it is an ideal core within which to further test IRD provenancing by magnetic signatures. By applying environmental magnetic analysis to samples from MD95–2006, this paper will address the following questions:

[13] 1. Can environmental magnetic analysis characterize IRD derived from different ice sheet sources in the sediments within MD95–2006?

[14] 2. Can magnetic unmixing models [e.g., *Thompson*, 1986] be used to estimate the proportions of IRD derived from different sources in IRD-rich layers within MD95–2006?

[15] 3. Can environmental magnetic analysis of MD95–2006 provide useful insights into the growth phases of the BIS during the period spanning GS16 to GS3, a period when terrestrial records of ice sheet growth/retreat are, at best, fragmentary?

[16] For the purposes of the following discussion, we define HLs as the intervals represented by the presence of LIS IRD and coeval with the HLs identified within the main IRD belt. IRD from ice sheets other than the LIS may contribute within the stadials, but do not dominate the HLs. We therefore refer to HLs as occurring within stadials (e.g., H4 occurs within GS9, but is not coeval with the entire GS9 interval). We use the interstadial numbering from the Greenland ice cores [after *Dansgaard et al.*, 1993; *Johnsen et al.*, 1992], with stadials numbered temporally following the interstadials [e.g., *Björck et al.*, 1998; *Walker et al.*, 1999]. We do not adopt the warm (W)/cold (C) scheme proposed for North Atlantic deep-sea cores by *McManus et al.* [1994], as their stadial numbering scheme contradicted the Greenland ice core scheme (see *Rousseau et al.* [2006] for discussion). Specific Bond cycles are labeled according to the HLs bounding them (e.g., the Bond cycle spanning GI12 to GI9 is referred to as the H5-H4 Bond cycle). We refer to ambient/background sediments as marine sediments deposited during cold phases, which do not contain abundant IRD.

3. Methods

3.1. Magnetic Measurements

[17] Dry, bulk sediments were subsampled at 1 cm contiguous intervals from core depths 1600 cm to 2850 cm (spanning MIS2 and MIS3) and were packed in 10 mL plastic pots. Nondestructive, rapid laboratory-induced magnetizations were then measured. Susceptibility (ratio of induced magnetization to magnetic field) was measured using a Bartington MS2 susceptibility meter with MS2B sensor. Artificial anhysteretic and isothermal remanent magnetizations (ARMs and IRMs) were grown using a Molspin alternating field (AF) demagnetizer (using a field of 100 mT) with an ARM attachment (coil producing a small direct field, here 0.04 mT) and a Molspin 1 T and a Magnetic Measurements 9 T pulse magnetizers respectively. All remanences were measured using a Molspin 1A magnetometer. Approximately 30 samples can be run per day. Hysteresis loops of selected subsamples were measured using a Molspin nuvo vibrating sample magnetometer using fields up to 500 mT, each loop taking approximately 20 min. Low-temperature remanent magnetization measurements were carried out on a further reduced selection of samples using a MPMS superconducting SQUID magnetometer, each sample taking approximately 5 hours to measure. The samples were cooled to 20 K, a remanent magnetization was then imparted using a 2.5 T field and the change in remanence was then monitored as the samples were warmed to 300 K. Natural samples tend to be mixtures of magnetic components, which can be challenging to fully identify and quantify, but can display significant relative differences. The

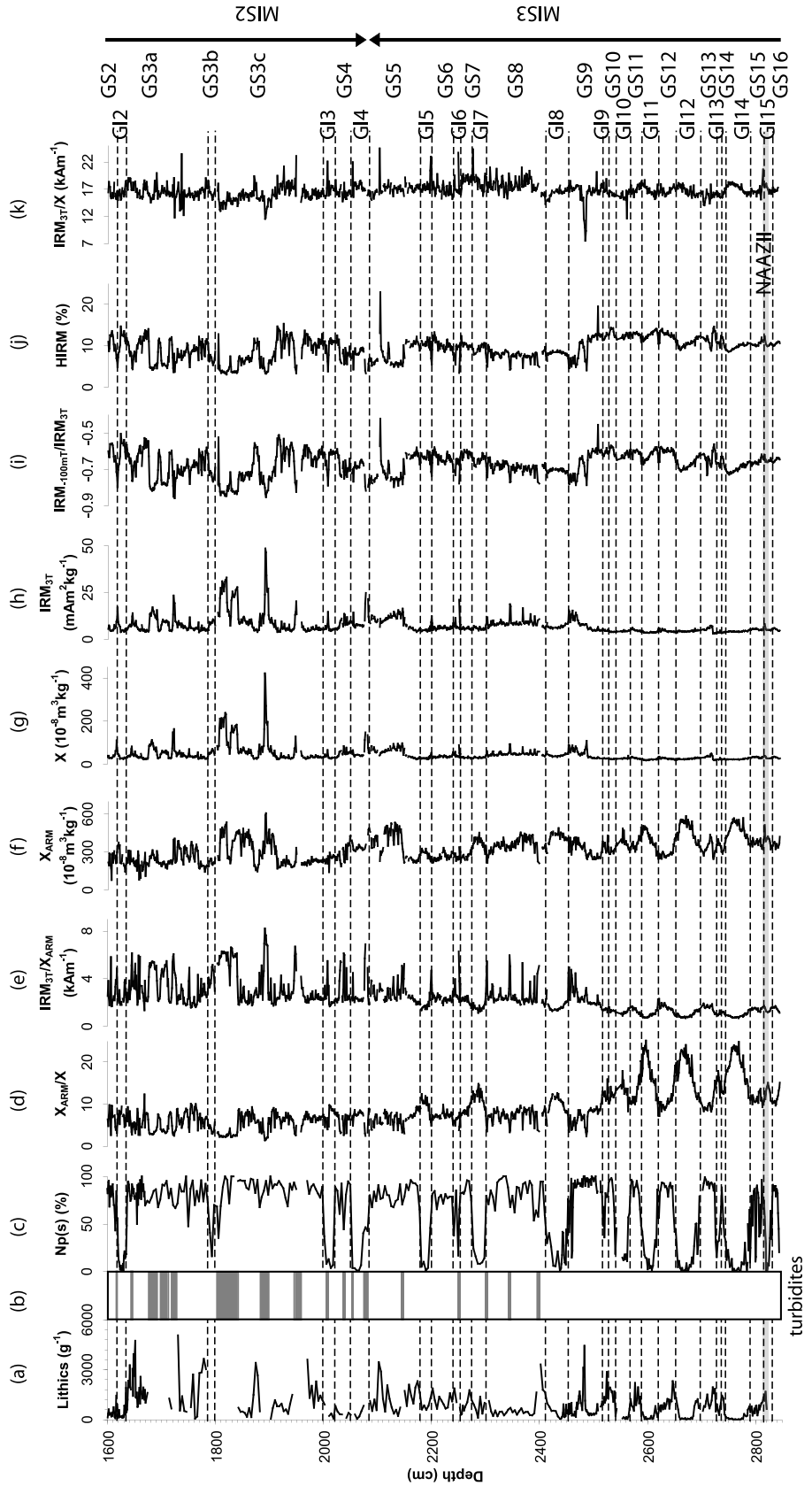

Figure 2. Profiles spanning GS16 to GS2. The lithic counts and *Np*(s) data (data compiled from *Austin et al.* [2004], *Dickson* [2004], and *Leigh* [2006]) were used to define the stadial/interstadial sequence. The shaded band at ~2817 cm represents the North Atlantic Ash Zone II. Eight magnetic parameters and ratios are shown reflecting IRD input and climatic variation.

measurements were selected to provide maximum information on magnetic concentration, magnetic domain state (linked to magnetic grain size) and magnetic mineralogy.

3.2. Interpretation of Environmental Magnetic Parameters

[18] Mass specific values of susceptibility (χ), ARM (usually expressed as a susceptibility (χ_{ARM}) by dividing the magnetization by the direct applied field, allowing comparison between measurements made in different laboratories [cf. *Sagnotti et al.*, 2003]) and IRM (here the IRM attained in the highest applied field namely 3 T) can indicate the concentration of ferromagnetic grains. *Peters and Dekkers* [2003, and references therein] showed some variation with grain size for χ and IRM for a given mineralogy. Larger differences do, however, exist between mineralogies e.g., the average χ for magnetite is 674×10^{-6} m^3 kg^{-1} in comparison to 0.97×10^{-6} m^3 kg^{-1} for haematite [*Peters and Dekkers*, 2003, and references therein]. In contrast, grains between 0.02 μm and 0.1 μm acquired significantly higher ARMs than larger grains [*Peters and Dekkers*, 2003, and references therein] and χ_{ARM} therefore gives an indication of single-domain ferrimagnetic grains. Normalizing χ_{ARM} by χ or IRM allows variations in magnetic grain size to be investigated. High (low) χ_{ARM}/χ and low (high) IRM/χ_{ARM} suggest the presence of single-domain (multidomain) grains. *Sagnotti et al.* [2003] warned that variations in experimental conditions could lead to misinterpretation when using the *King et al.* [1982] biplot of ARM versus susceptibility for grain size determination. IRM ratios (here we use IRM_{-100mT}/IRM_{3T}) allow variations in domain state and/or mineralogy to be identified. For a given mineralogy lower values suggest larger grains. Values approaching -1 suggest the presence of easily magnetized grains (e.g., magnetite) whereas values approaching +1 suggest hard to magnetize grains (e.g., haematite). The proportion of the IRM_{1T} attributed to magnetically hard grains e.g., haematite or goethite, often referred to as the hard IRM (HIRM), was determined following *Liu et al.* [2002] and *Watkins* [2003], by dividing the AF demagnetization (100 mT) of IRM_{1T} by IRM_{1T} and expressing as a percentage.

[19] Hysteresis loops contain a wealth of magnetic information. The height of the loop gives an indication of concentration and, using the low and high field gradients, can be divided in to ferromagnetic and paramagnetic contributions. For a given mineralogy the width of the loop at zero magnetization (coercivity) indicates domain state. High values suggest single domain and low values multidomain (low values can also indicate very fine <0.03 μm superparamagnetic grains). Coercivity can also vary with mineralogy. Magnetite has average coercivities of 9.8 mT and haematite 268 mT [*Peters and Dekkers*, 2003, and references therein].

[20] Low-temperature remanent magnetization curves can confirm the presence of certain minerals, which display low-temperature crystallographic phase transitions and isotropic points. For example, magnetite displays a crystallographic phase transition (change between inverse cubic spinel and monoclinic structures) at 110–120 K, known as the Verwey transition [e.g., *Verwey and Haayman*, 1941]. Magnetite also displays an isotropic transition (change in magnetocrystalline anisotropy and easy directions of magnetization) at ~130 K (T_i) [e.g., *O'Reilly*, 1984]. The decrease in remanence as magnetite is warmed through the Verwey transition is greater in multidomain grains than single-domain grains [*Özdemir et al.*, 1993]. Partial oxidation of magnetite can lower the Verwey transition temperature and with, e.g., maghemitization, the transition can be suppressed [*Özdemir et al.*, 1993]. For multidomain titanomagnetites ($Fe_{3-x}Ti_xO_4$, $0 \leq x \leq 1$) *Moskowitz et al.* [1998] showed for $x < 0.4$ large drops in remanence below 100 K, with little change above the transition temperature; the behavior is associated with isotropic points. For $x > 0.4$ the remanences are temperature independent below 50 K, the remanences drop between 50 K and 80 K, with further gradual decreases between 80 K and 300 K; the behavior is associated with anisotropy constants. Other minerals displaying low-temperature transitions include haematite (Morin transition at ~263 K [e.g., *Morin*, 1950; *de Boer et al.*, 2001]) and pyrrhotite (iron sulphide) (transition at 30–34 K [e.g., *Dekkers et al.*, 1989]).

3.3. X-Ray Diffraction

[21] Approximately 1 g of crushed sediment was packed into standard Philips sample holders and run in a Philips PW1050/Hiltonbrooks DG2 instrument using a cobalt anode tube. The data were analyzed with WinXRD version 2 software using the ICDD powder diffraction file. Quantification of mineral percentages was carried out using SiroQuant version 3.

4. Results

[22] Figure 2 displays profiles spanning 2850 cm to 1600 cm (GS16 to GS2) in MD95–2006. The grain counts (>150 μm) (Figure 2a) and *Np*(s) percentages (Figure 2c), with a resolution of 2–4 cm are compiled from *Austin et al.* [2004], *Dickson* [2004] and *Leigh* [2006]. The MD95–2006 record was tied to the Greenland ice core (GISPII) record by the presence of the NAAZII ash at ~2817 cm [*Austin et al.*, 2004] (Figure 2). Transition mid points in the *Np*(s) record (Figure 2c) were used to define warm/cold intervals. While this approach is generally very robust, there is some ambiguity in assigning the Greenland Interstadial (GI) numbering to the *Np*(s) record for MD95–2006. For example, there is a warming in the MD95–2006 record between GI3 and GI2, which is not numbered in the $\delta^{18}O$ ice record of *Dansgaard et al.* [1993]. We have labeled the warming as GS3b, following the scheme recommended by *Björck et al.* [1998]. An unnumbered warming within GS3 was also evident in the record of *Moreno et al.* [2002] from core MD95–2042 off the Portuguese Margin; H2 was positioned between the unnumbered warming and GI2. *Moros et al.* [e.g., 2002, 2004] have also identified three warm intervals between GI5 and GI2 in cores from the Reykjanes Ridge. They, however, have labeled the warm intervals as 4b, 4a and 3, in contrast to our GI4, GI3 and GS3b. Other features in the *Np*(s) record of MD95–2006 include fluctuations, which make positioning of the GS9/GI8 boundary difficult, a short warm interval is present at the end of GS13 and a number of warm intervals are observed within GS15. The approximate position of the MIS3-2 boundary is also indicated in Figure 2. *Wilson and Austin* [2002] placed the boundary at 30 ka B.P. and

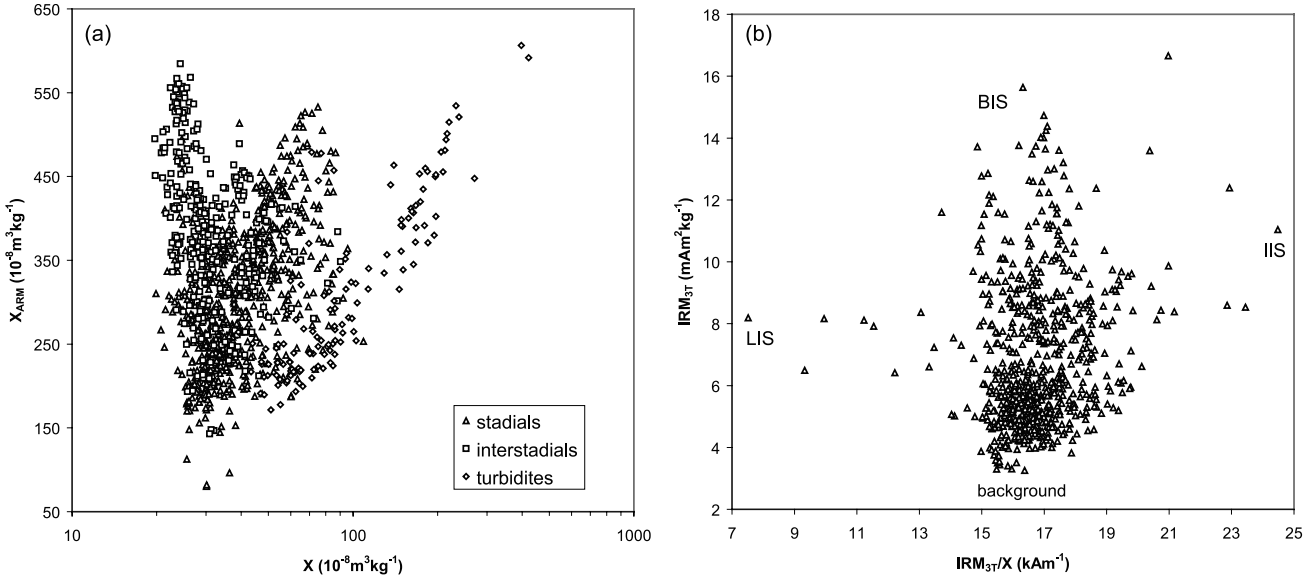

Figure 3. (a) χ_{ARM} versus χ for stadial, interstadial and turbidite samples from GS16 to GS2. Following plotting method of *Kissel* [2005] revealing three trends suggesting differences in magnetic grain size and/or mineralogy as well as concentration. (b) IRM_{3T} versus IRM_{3T}/χ for the stadial samples shown in Figure 3a.

given their age-depth model, the depth was approximately 2070 cm, between GS5 (containing H3) and GI4 (Figure 2).

[23] The grain count data (Figure 2a) are compiled from *Austin et al.* [2004], *Dickson* [2004] and *Leigh* [2006] and represent the concentration of grains > 150 μm. In many marine cores within the IRD belt, the concentration of grains in this size fraction is taken as an indication of IRD input. However, in MD95–2006, *Knutz et al.* [2001] observed a number of intervals within the core containing turbidite sediments on the basis of visual inspection of the sediments and their well sorted/fining upward properties (Figure 2b). Because of differences in the IRD grain counts between Figure 2a (>150 μm) and *Knutz et al.* [2001] (250–500 μm), direct comparisons in IRD records are not possible. The grain count data for the turbidite layers are excluded from Figure 2a, which should, therefore, represent coarse-grained input derived from IRD sources rather than other depositional processes. The turbidite layers were, however, subjected to magnetic analysis and, as discussed more fully below, show a distinct magnetic composition compared with the layers dominated by IRD and which would be difficult to explain by processes of sediment reworking and particle size sorting.

[24] Figures 2d, 2e, 2f, 2g, 2h, 2i, 2j, and 2k show various magnetic parameters and ratios. The χ_{ARM}/χ ratio (Figure 2d) and χ_{ARM} (Figure 2f) seem to follow the D-O pacing of the *Np*(s) data (Figure 2c) during MIS3. The correlation between the magnetic parameters and *Np*(s) is seen particularly clearly in the χ_{ARM}/χ data during the H5-H4 Bond cycle (GS13-GS9). A nonparametric correlation between *Np*(s) and χ_{ARM}/χ for the H5-H4 interval is statistically significant ($r_s = 0.708$). *Np*(s) is widely accepted as a proxy for sea surface temperatures [*Pflaumann et al.*, 2003], suggesting an association between χ_{ARM} (or ratios derived from it) and the "on/off" pattern of stadial/interstadial transitions associated with the rapid south/north migration of the oceanic polar front at this latitude in the NE Atlantic.

[25] Figures 2i, 2j, and 2k show magnetic parameters reflecting variations in magnetic mineralogy and/or grain size. The turbidite intervals (Figure 2b) are recognized as troughs in IRM_{-100mT}/IRM_{3T} (Figure 2i) and HIRM (Figure 2j), which coincide with peaks in χ (Figure 2g) and IRM_{3T} (Figure 2h), indicating the intervals of high magnetic concentration are also magnetically softer, suggesting different sources of magnetic grains. During the stadials in the H5-H4 Bond cycle variability in IRM_{-100mT}/IRM_{3T} (Figure 2i) and HIRM (Figure 2j) values are largest during GS9 and GS13, containing H4 and H5. The IRM_{3T}/χ in Figure 2k shows an interval of very low values during GS9 attributed to H4. IRM_{-100mT}/IRM_{3T} (Figure 2i) and HIRM (Figure 2j) (reflecting proportions of hard magnetic minerals e.g., haematite) show an interesting long-term trend following the Bond cycles. A shift to low values coincides with stadials containing HLs. During the following Bond cycle the parameters show an increasing trend through successive stadials. A similar trend was hinted at in the percentage of haematite stained grains in the records of *Bond et al.* [1999].

4.1. IRD Compositional Variability

[26] The compositional variability of the MD95–2006 sediments is illustrated further via two biplots (Figure 3). Figure 3a plots χ and χ_{ARM} and the samples essentially fall into three overlapping clusters. Samples from the interstadial periods (open square symbols) show the lowest χ values but variable χ_{ARM} and limited covariance of the two magnetic properties ($r = -0.302$). In contrast, samples from the stadial stages tend to show higher χ values and these covary with χ_{ARM} ($r = 0.502$). Samples from the turbidite layers form the third cluster showing the highest χ

values and a clear relationship between χ and χ_{ARM} (r = 0.883). All these correlations are significant at the 95% confidence level. This clustering suggests distinct magnetic compositions for the three types of samples. Moreover, given the different trends between χ and χ_{ARM} within the three clusters, the differences cannot be explained solely by magnetic concentration variation; magnetic grain size and/or mineralogy must also be distinct.

[27] The differences between the interstadial and stadial samples is most easily explained by more active IRD deposition during the stadial stages with the IRD composition reflecting that of the assemblage of source rocks from which it is derived and their addition to the ambient cold-stage marine sediment. While this is likely, it is also true that some IRD deposition does occur within the interstadial stages and that there are periods during stadials with little or no IRD deposition. This would help to explain the overlap between these two clusters and their convergence toward the bottom left of Figure 3a. However, a further factor is also involved as preliminary TEM examination of magnetic mineral extracts from both stadial and interstadial samples shows the presence of biogenically produced magnetite within the interstadial samples, which is absent from the stadial samples. The presence of such ultrafine-grained (0.1 μm) magnetite would explain the higher χ_{ARM} values in some interstadial stage samples. Given the strong correlation of the *Np*(s) and χ_{ARM}/χ ratio (Figures 2c and 2d respectively), it is tempting to suggest that this ratio reflects the contribution of biogenically derived magnetite which, in turn, is related to a climatic control.

[28] The distinct properties of the turbidites (in Figure 3a) could be explained in a number of ways. If, for example, these sediments represented reworking of preexisting IRD-rich marine sediments, their different magnetic properties may result from particle size (density-based) sorting of the sediment during reworking. However, magnetic analysis of the >150 μm fraction of the nonturbidite IRD-rich layers within MD95–2006 suggests that they do not contain the same magnetic mineral assemblage as the turbidites. This suggests that the original sediments from which the turbidites were reworked were not compositionally similar to the IRD-rich layers within MD96–2006 and, presumably, must have been derived from a different assemblage of source rocks.

[29] While the differences between the turbidites and stadial samples (sediment source driven?) and the interstadial and stadial samples (climatically driven?) are interesting in their own right, the focus of this paper is on the provenance of the IRD within MD95–2006 and whether this might provide information about the behavior of the BIS. We acknowledge that IRD occurs outside these stadial intervals, but the discussion below will concentrate upon the magnetic properties of the stadial stage samples where, in the main, the highest IRD concentrations are observed (Figure 2a).

[30] Magnetic variation within the stadial samples is shown by the biplot of IRM_{3T} (predominantly controlled by magnetic concentration) and IRM_{3T}/χ ratio (indicative of magnetic grain size and/or mineralogy) (Figure 3b). Figure 3b can be used to identify a number of extremes of magnetic behavior and four are indicated upon the plot, with extreme low and high values of both IRM_{3T}/χ and IRM_{3T}. Further biplots, combining different magnetic parameters, produced similar patterns to Figure 3b, with the same samples consistently being identified as the extremes within the data space.

[31] In order to clarify and confirm the different magnetic properties of the various extreme types identified in Figure 3b, hysteresis loops and low-temperature remanent magnetizations were analyzed. Figure 4 shows hysteresis loops of the four extremes in Figure 3b, and also a turbidite sample for comparison. With the exception of the hysteresis loop of the individual grain in Figure 4c, the hysteresis loops were measured on bulk samples. Figure 4b exhibits the lowest coercivity (width of loop); Figure 4d has the highest paramagnetic component; Figure 4e has the highest magnetic concentration. The hysteresis loop of the individual grain (of basaltic origin) shown in Figure 4c has a very high coercivity and high magnetization. Figure 5 shows the low-temperature remanent magnetization curves for nine samples. A loss in remanence at ~120 K for all samples is indicative of the Verwey transition and indicates the presence of (titano)magnetite. Sample 2486–2487 cm (lowest IRM_{3T}/χ in Figure 3b; Figure 4b) shows the largest drop in remanence indicating the presence of stoichiometric, multidomain magnetite grains. The drop in remanence before 100 K and suppression of the transition exhibited by 1819–1820 cm, 1891–1892 cm and 2145–2146 cm in Figure 5 suggests partially oxidized pseudo-single-domain (titano)-magnetite. The other five samples shown in Figure 5 are characterized by intermediate drops in remanence before 100 K and extreme suppression of the transition, which could be indicative of partially oxidized single-domain (titano) magnetite.

[32] *Stoner et al.* [1996] have defined the magnetic properties of HLs. The detrital carbonate layers in core P-094 (Labrador Rise) (Figure 1) displayed peaks in susceptibility and troughs in IRM. The detrital carbonate layers were also characterized by low coercivity and the presence of the Verwey transition indicative of multidomain magnetite. *Walden et al.* [2007] demonstrated similar magnetic properties in LIS IRD from IRD-rich layers associated with H1 and H2 in core OMEX-2K on the Goban Spur (off SW Britain). These magnetic properties are exhibited by an interval at ~2486 cm in MD95–2006 (earliest χ peak in GS9 in Figure 2g, with no corresponding IRM_{3T} peak in Figure 2h, magnetically soft with lowest IRM_{3T}/χ values in Figure 3b, low coercivity hysteresis loop in Figure 4b and low-temperature remanent magnetization curve with Verwey transition in Figure 5) coinciding with the presence of dolomitic carbonate shown by *Knutz et al.* [2001] and *Leigh* [2006]. These magnetic properties characterize the presence of LIS IRD in GS9 in MD95–2006.

[33] The samples with extremely high IRM_{3T}/χ values in Figure 3b are magnetically hard, which is confirmed by the high coercivity shown by the hysteresis loop in Figure 4c. The individual grain measured was of basaltic origin. The NAAZII peak (2816–2817 cm) has an IRM_{3T}/χ ratio of 20.6 kA m^{-1}, plotting toward the right of Figure 3b. We suggest the magnetically hard samples represent an Icelandic-derived source.

[34] The samples with high IRM_{3T} values and intermediate IRM_{3T}/χ ratios also exhibit high susceptibilities (Figure 2g) and intermediate coercivities (Figure 4a).

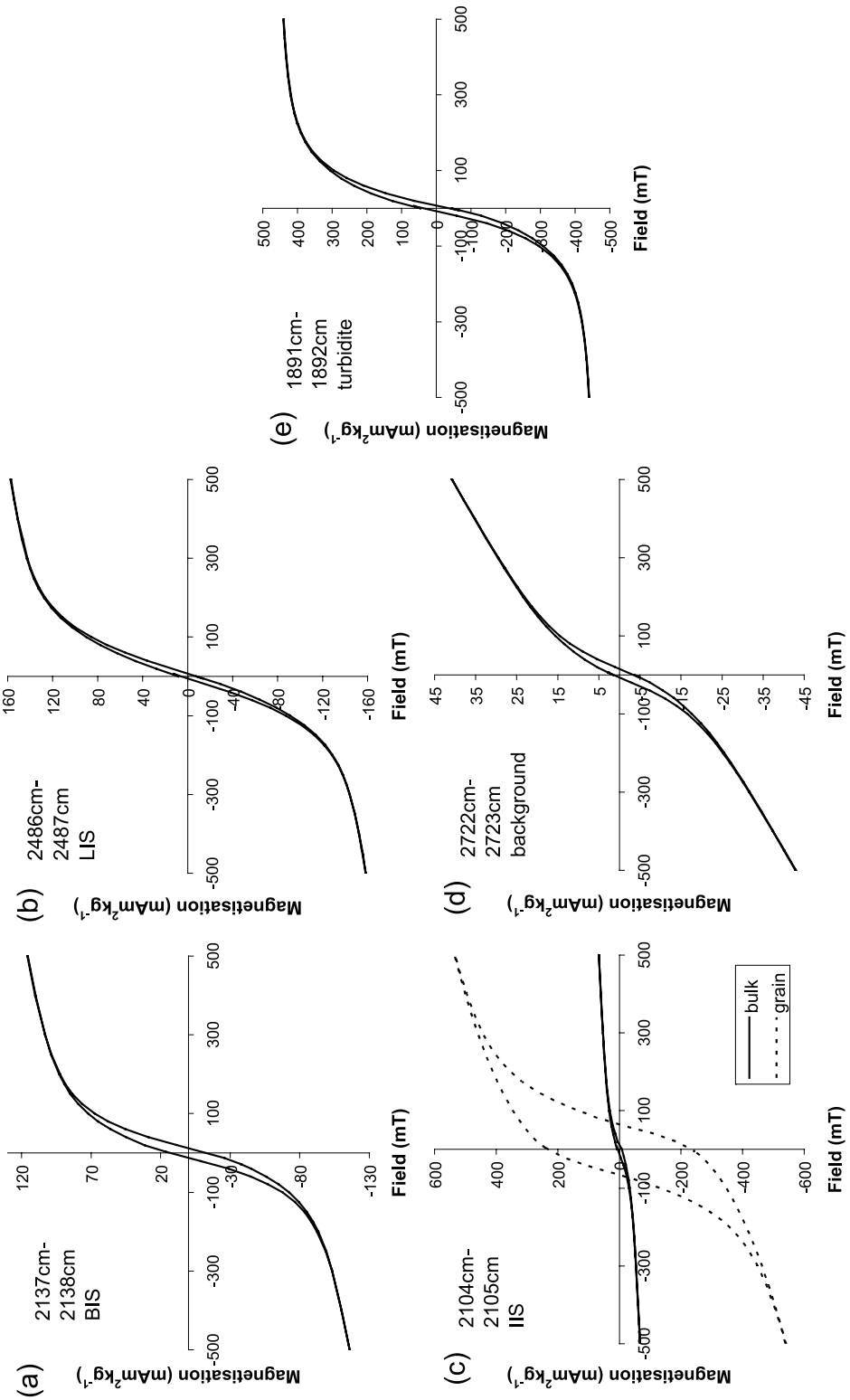

Figure 4. Hysteresis loops showing differences in ferrimagnetic and paramagnetic components for the four types of magnetic behavior indicated in Figure 3b: (a) BIS, (b) LIS, (c) IIS (including a hysteresis loop measured on a single grain exhibiting high coercivity), (d) background and also (e) a turbidite sample for comparison.

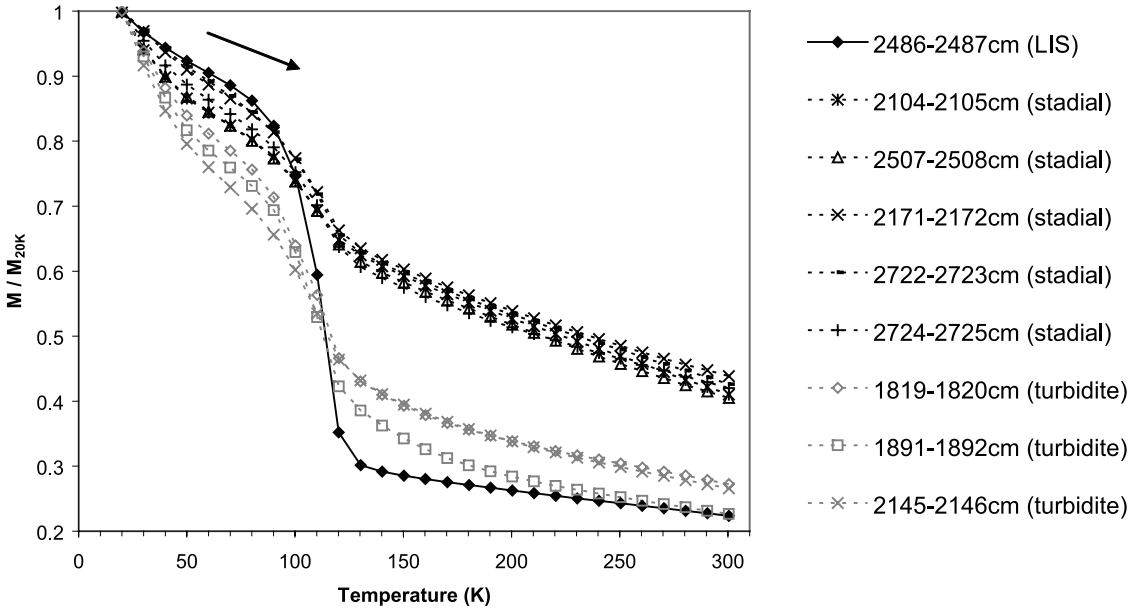

Figure 5. Low-temperature remanent magnetization curves measured by cooling the samples to 20 K, imparting a remanent magnetization using a field of 2.5 T and then monitoring the remanence during warming to 300 K. The remanent magnetizations (M) are normalized by the remanent magnetization induced at 20 K (M_{20K}). The curves represent LIS IRD, five non-LIS stadial samples and also three turbidite samples for comparison.

Samples exhibiting these magnetic properties show a positive relationship with the IRD concentrations (Figure 2a). Given the location of MD95–2006 on the Barra Fan and the previous work published on the core [e.g., *Kroon et al.*, 2000; *Knutz et al.*, 2001; *Wilson and Austin*, 2002; *Wilson et al.*, 2002], it is highly likely that the IRD deposition is dominated by material derived from the NW margins of the BIS. We therefore suggest that these magnetic properties are characteristic of IRD derived from the BIS.

[35] The magnetic analyses were performed upon bulk samples (not just the > 150 μm fraction used for the lithic counts in Figure 2a) and will therefore also contain a "background" signal representative of the ambient marine sediment when IRD concentrations are relatively low. We suggest that the extremely low IRM_{3T} values, with intermediate IRM_{3T}/χ ratios, shown in Figure 3b, represent the background signal. Table 1 summarizes representative magnetic data for the three identified IRD sources, the background and turbidite signals.

4.2. X-Ray Diffraction

[36] Independent confirmation of the differences shown by the four magnetic types in Figure 3b was provided by X-ray diffraction. Table 2 lists the mass percentages of one sample per type. The LIS sample is characterized by the highest dolomite and lowest quartz proportions. The Icelandic and background samples display similar X-ray diffraction properties, with high clay components. The background sample has the lowest feldspar proportion of the five analyzed samples. The BIS sample has high quartz and low calcite and clay proportions. Also included in Table 2 is a turbidite sample for comparison. It has similar proportions to the BIS, but has the lowest clay and calcite and highest feldspar and quartz proportions of the analyzed samples.

4.3. Quantifying IRD Input From Different Sources

[37] Using the linear additivity of mass specific magnetic data [e.g., *Carter-Stiglitz et al.*, 2001], estimates can be made of different components (end-members) within a given measured sample. The components can be either (1) magnetic end-members (i.e., multidomain magnetite, single-domain greigite, etc.) [e.g., *Thompson*, 1986; *Peters*, 1995; *Carter-Stiglitz et al.*, 2001] or (2) source end-members showing distinct magnetic properties between the sources (e.g., *Yu and Oldfield* [1989], *Shankar et al.* [1994] (combining magnetic and radiogenic data), and *Peters and Turner* [1999]). Here we assume the four types of extreme magnetic behavior shown in Figures 3b, 4 and 5 and in Tables 1 and 2 are four potential sediment sources and we estimate their proportions within the stadial phases of the record (as shown in Figure 2). These end-members

Table 1. Magnetic Data for MD95–2006 for the Three Identified IRD Sources, the Background and Turbidite Signals[a]

	LIS (2486–2487 cm)	IIS (2104–2105 cm)	BIS (2137–2138 cm)	Background (2722–2723 cm)	Turbidite (1891–1892 cm)
χ (10^{-8} m^3 kg^{-1})	109	45	96	21	422
IRM_{3T} (mA m^2 kg^{-1})	8.2	11.0	15.6	3.3	48.6
IRM_{-100mT}/IRM_{3T}	−0.79	−0.42	−0.79	−0.56	−0.84
IRM_{3T}/χ (kA m^{-1})	7.5	24.5	16.3	16.0	11.5

[a]IRD, ice-rafted debris; LIS, Laurentide ice sheet; IIS, Iceland ice sheet; BIS, British ice sheet; IRM, isothermal remanent magnetization.

Table 2. Quantitative X-Ray Diffraction Analyses of the Three IRD Types and Background Signal Indicated in Figure 3b[a]

Type	Quartz	Calcite	Dolomite	Feldspar	Clay	Halite	Pyrite
LIS (2486–2487 cm)	19	27	13	19	22	0	0
IIS (2104–2105 cm)	24	20	2	11	41	1	1
BIS (2137–2138 cm)	42	12	3	19	22	2	0
Background (2722–2723 cm)	23	23	3	6	44	1	0
Turbidite (1819–1820 cm)	43	8	1	28	17	2	1

[a]Analyses were performed using SiroQuant version 3. A turbidite sample (Figure 3a) is also included. The values given are mass percentages.

were used to construct an "unmixing" model in Microsoft's Excel XP using the Solver Add-In and on the basis of the principles outlined by *Thompson* [1986] and *Walden et al.* [1997]. This model allowed the proportions of each source to be quantified for each stadial sample within the core.

[38] The model construction is based upon: p, the number of magnetic parameters used in the modeling procedure; e, the number of end-members (sources) used in the modeling procedure; a_{ij}, the measured value of magnetic parameter j in end-member (source) i; b_j, the measured value of magnetic parameter j in the natural sample being modeled; x_i, the hypothetical proportion of end-member i in the natural sample where $x_i \geq 0$ and $x_i \leq 1$ and s_j, the simulated (modeled) value of magnetic parameter j in the simulated version of the natural sample where $s_j = \sum_{i=1}^{e} a_{ij}\, x_i$. The minimum difference between the simulated and natural samples is found by minimizing

$$\sum_{j=1}^{p}\left(\sum_{i=1}^{e} a_{ij}x_i - b_j\right)^2 = \sum_{j=1}^{p}\left(s_j - b_j\right)^2 \qquad (1)$$

subject to the constraint that $x_i \geq 0$ and $x_i \leq 1$ for each end-member i and $\sum_{i=1}^{e} x_i = 1$.

[39] The model used a combination of the concentration-dependent mass specific χ, IRM and demagnetization data as, at the relatively low concentrations of magnetic minerals found in most natural sediments, these are linearly additive. The ARM data was not included because of its climatic response. Each stadial sample was unmixed to give an estimate of the proportion of each of the four end-members (i.e., LIS, IIS, BIS and background, as shown in Figure 3b).

[40] The output from the model is summarized in Figure 6. For a number of reasons (in particular, the somewhat subjective nature by which end-member samples are selected), the proportions of each end-member ascribed to a particular sample must be considered as semiquantitative estimates [*Walden et al.*, 1997]. However, the modeled IRM_{3T} and measured data match closely (Figure 6a), suggesting the model is mathematically robust and that, in mathematical terms at least, it is possible to unmix the majority of the stadial samples on the basis of the four end-member types identified. Figures 6b, 6c, 6d, and 6e show the proportions of the four end-members allocated by the model with age.

[41] The LIS proportions (Figure 6b) are, overall, the lowest of all the four sources. The one exception is during GS9, constrained by high dolomitic grain counts and assigned to H4, where it dominates for a short period. The NAAZII peak (2816–2817 cm) has an IIS proportion of 0.24 (Figure 6c). Peaks of IIS proportions of similar or higher values occur during GS13, GS9, GS5, each of which contains an HL. The BIS proportions dominate during the H3-H2 Bond cycle. There is a significant input from the BIS toward the end of GS9, following H4. The background source is the most abundant throughout the analyzed section of the core, except during the later stages of GS9, GS5 and GS3c.

[42] Figure 7 shows the unmixing results for GS7-GS9 in more detail. The four sources are plotted on a common axis for each stadial to allow comparison between the proportions. In Figure 7c during GS9, pre H4, the background signal dominates, with the exception of one peak of IIS. During H4 the background signal falls to zero. Following H4 the background increases for a period and then decreases again, coinciding with an increase in BIS proportions. Following through the H4-H3 Bond cycle, the BIS proportions at the end of GS9 average 0.68, during GS8 (Figure 7b), they average 0.41 and during GS7 (Figure 7a), they average 0.16. A similar sequence of decreasing BIS proportions is observed from post-H3 GS5 (average of 0.65), through GS4 (average of 0.36) and the early stage of GS3c (average of 0.12) (Figure 6d).

5. Discussion

5.1. Comparison to North Atlantic and Nordic Seas Cores

[43] The biplot of χ_{ARM} versus χ in Figure 3a follows the data presentation of *Kissel* [2005] allowing comparison between the magnetic properties of core MD95–2006 and a number of other cores from the North Atlantic and Nordic Seas. *Kissel* [2005] has distinguished two magnetic signatures:

[44] 1. In cores from the Ruddiman IRD belt (40–55°N) the magnetic properties responded to the deposition of HLs. Samples were scattered on the biplot of χ_{ARM} versus χ, with differences observed in magnetic concentration and magnetic grain size/mineralogy (high concentrations of coarse, multidomain magnetite grains were present during HLs with lower concentrations of finer magnetic grains in the sediment intervals between the HLs).

[45] 2. In cores along the path of the North Atlantic Deep Water (NADW) in the Nordic Seas the magnetic properties responded to the D-O cycles. Samples plotted linearly on the biplot of χ_{ARM} versus χ, with variation only in magnetic concentration (high magnetic concentration during the warm events and low during the cold events).

[46] The scattered pattern in Figure 3a indicates variation in magnetic concentration and magnetic grain size/mineralogy for the MD95–2006 samples. The range of χ_{ARM} values exhibited by the interstadials in Figure 3a suggest a similar pattern to (2) above. Although MD95–2006 is not located within the Ruddiman belt the different χ_{ARM} to χ trends of the stadial samples compared to the

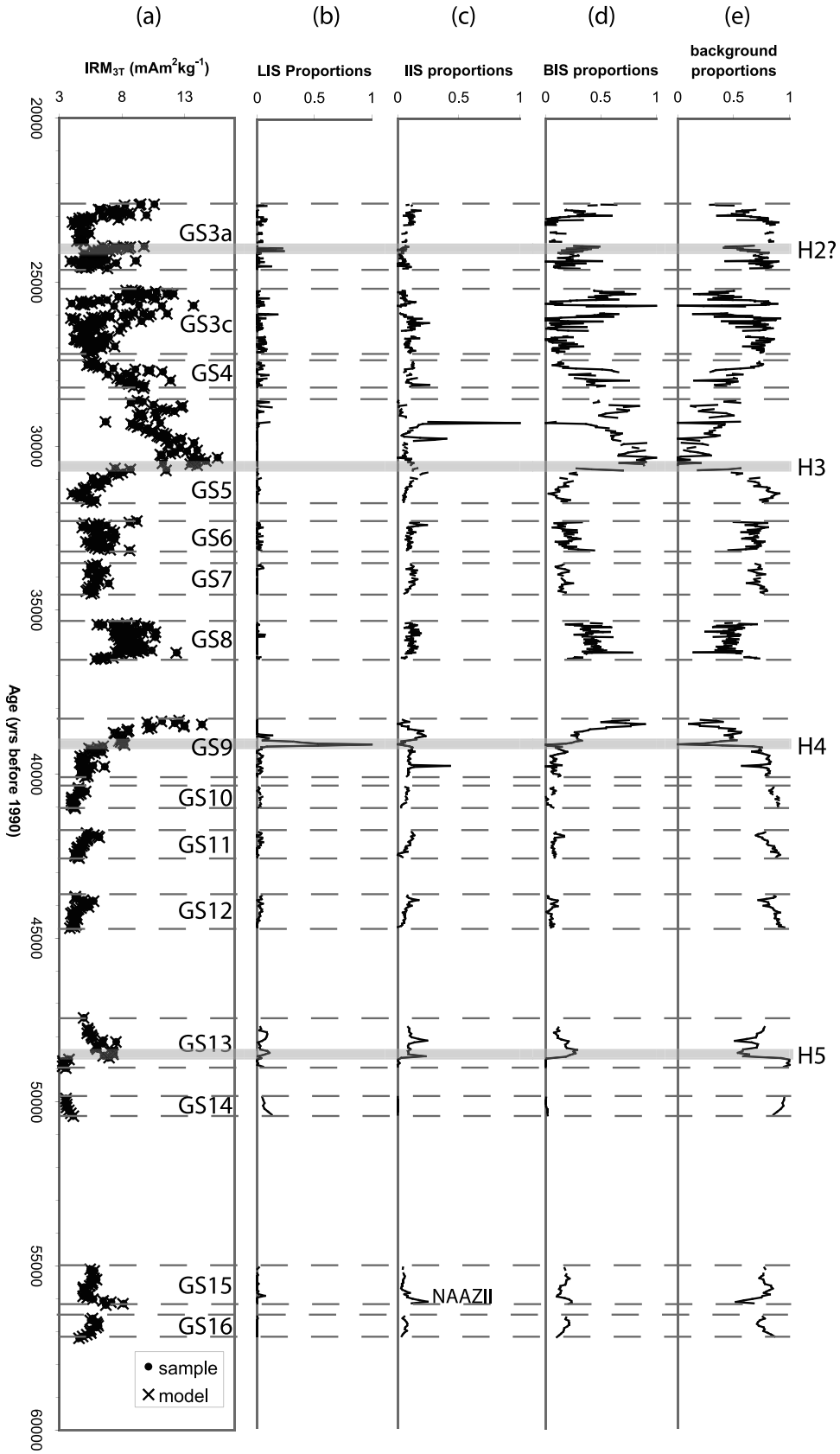

Figure 6. Magnetic unmixing results for stadial samples from GS16 to GS3a; (a) measured (dot) and model (cross) data for IRM_{3T} showing the goodness of fit and (b) LIS, (c) IIS, (d) DIS, and (e) background proportions estimated for each of the four sources within each stadial sample.

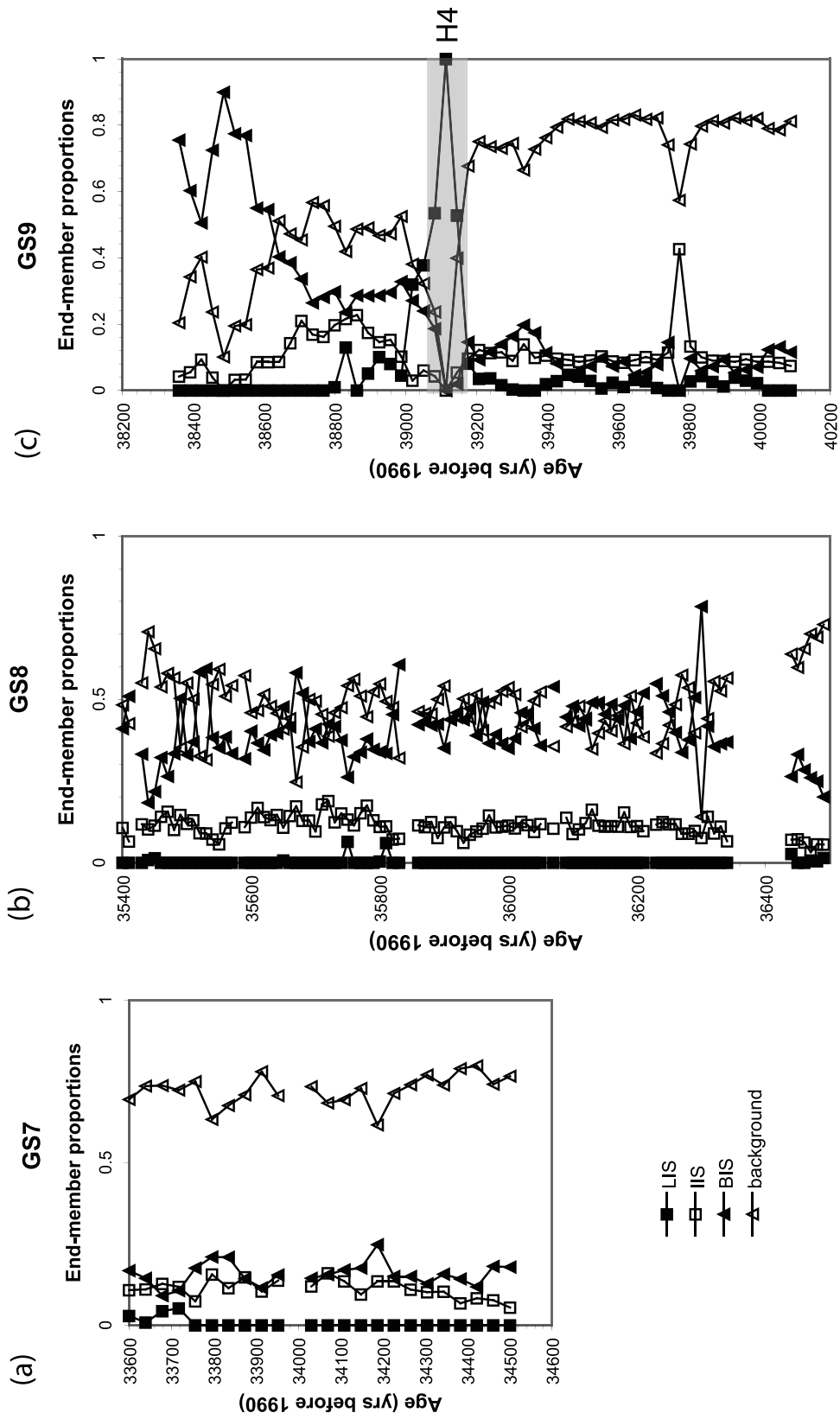

Figure 7. Details of the unmixing results shown in Figure 6 for GS7, GS8 and GS9 showing comparisons between the source proportions and phasing within the stadials.

interstadial samples in Figure 3a suggest input from different sources similar to (1) above. We propose that the lithic input of IRD from the nearby BIS to core MD95–2006, which has a distinct magnetic signal from the ambient background sediment, results in the observed variation in magnetic grain size/mineralogy.

[47] *Richter et al.* [2001] have interpreted high susceptibilities in their core from the Feni Drift, Rockall Trough, as input of IRD from the LIS. On the basis of our findings of IRD from the NW BIS also exhibiting high susceptibility, we suggest the high susceptibilities of *Richter et al.* [2001] could be attributed to input from the BIS rather than from the LIS.

5.2. Pattern of IRD Deposition

[48] *Knutz et al.* [2001] first suggested, on the basis of concentrations of basaltic material from the British Tertiary Province within MD95–2006, that the BIS fluctuated and delivered IRD in time with the D-O cycles. They also noted an abrupt increase in the basalt concentration at 30 ka B.P., coinciding with the MIS3-2 transition. Similarly, *Wilson and Austin* [2002] observed a change in lightness and reflectance at the MIS3-2 transition, with D-O cycles clearly seen in the record prior to the transition and shorter periodicities after the transition during the expansion of the BIS to its maximum extent.

[49] On the basis of the above interpretation of the various end-members used in the magnetic unmixing, it is possible to make some further inferences about the pattern of IRD deposition throughout the period GS16 to GS2 in MD95–2006. With the exception of H4 during GS9, the LIS IRD appears to make only minor contributions to the total IRD received at the MD95–2006 core site, with little or no LIS IRD identified during the stadials coeval with the other HEs. Such a pattern is consistent with H4 being the largest of the HEs [*Hemming*, 2004] and there being a significantly reduced BIS IRD input at this time during MIS3. In contrast the overwhelming input of BIS IRD during GS3a masks the H2 LIS IRD input. We have tentatively marked the highest proportion of LIS during GS3a as H2 in Figure 6.

[50] Comparison between the IRD concentration data (Figure 2a) and the proportion of the BIS end-member (Figure 6c) ascribed by the model reveals some interesting features. As noted earlier, the IRD concentration data suggests, with the exception of some minor peaks, IRD deposition was at generally low levels until the end of GS5 (containing H3 and the MIS3-2 transition). Between H5 and H4, low lithic counts are mirrored by low proportions of BIS IRD, suggesting that the BIS was not able to deliver significant amounts of IRD into the marine system. However, while the IRD concentrations stay at low levels through the H4-H3 Bond cycle, the proportions of BIS IRD are higher. While the relationship between IRD delivery and ice sheet size is complex [*Andrews*, 1998], the obvious inference from these data would be BIS expansion during H4-H3, prior to the MIS3-2 transition. On the basis of terrestrial records, little is known about the development of the BIS during MIS3 and, while there are a number of significant assumptions inherent in the argument made here, it does suggest some considerable potential for magnetic characterization of IRD to provide information on the timing of individual ice sheet growth. After GS5 (containing H3), both the IRD concentrations and the proportion of BIS IRD show marked increases, suggesting further BIS expansion at around 30 ka B.P., consistent with other evidence of the development of the BIS and the concept of global ice expansion during MIS2.

[51] From Figures 6 and 7 we can get an insight into IRD sequencing surrounding HLs. Prior to H4 in GS9 the background signal is dominant, with no evidence of a BIS precursor. Following H4 BIS IRD dominates. Within GS9 there are also pulses of IIS prior to and following H4. Within GS5 (containing the atypical H3) following the initial dominance of the background signal the sequence follows pulses of BIS IRD, IIS IRD, and then BIS IRD again. GS5 contains the highest proportions of IIS IRD. Following the positioning of H2 in Figure 6, pulses of BIS IRD are evident prior to and following H2.

6. Conclusions

[52] Mineral magnetic measurements of bulk Barra Fan sediments from core MD95–2006 have shown: discrimination between several IRD sources using e.g., isothermal remanent magnetizations, hysteresis loops and low-temperature transitions; association between anhysteretic remanent magnetizations and the "on/off" pattern of Dansgaard-Oeschger cycles reflecting the rapid migration of the oceanic polar front over the core site; trends in proportions of hard magnetic minerals reflecting the longer-term Bond cycles.

[53] IRD from the LIS present in MD95–2006 is characterized by high susceptibility (χ) with correspondingly low IRM, low coercivity and presence of the Verwey transition indicative of multidomain magnetite (in agreement with *Stoner et al.* [1996]). IRD from the IIS is characterized by high coercivity. The magnetic signal of IRD deposited by the BIS, off the NW coast of Scotland, is characterized by high χ and correspondingly high IRM, medium coercivity and suppressed Verwey transition suggesting partially oxidized single-domain magnetite. The ambient hemipelagic sediment background signal during the stadials of the last glacial is characterized by low χ and IRM. The distinct characteristics of the IRD from different sources allowed development of a magnetic unmixing model to quantify proportions of each source within each stadial sample from GS3a to GS16. The IRD discrimination could be developed further by combining the magnetic data with radiogenic isotopic analysis as shown by *Walden et al.* [2008] for sediments from the Goban Spur, off SW Britain.

[54] Magnetic unmixing in terms of potential IRD sources showed an increase in proportions of BIS IRD at the MIS3–2 transition (also observed by *Knutz et al.* [2001] and *Wilson and Austin* [2002]), but also suggested BIS IRD deposition during MIS3, from the end of GS9. This is the first provenance data suggesting that BIS expansion occurred within MIS3, probably as early as 38.5 ka B.P. LIS IRD was only found to be dominant during GS9, namely H4 (confirmed by the presence of dolomitic carbonate [*Knutz et al.*, 2001; *Leigh*, 2006]) and is overwhelmed by BIS IRD surrounding H2 as a result of BIS expansion across the continental shelf off NW Scotland.

[55] **Acknowledgments.** The research was supported by the Leverhulme Trust (grant F/00 268/N) and NERC (grant NER/A/S/2001/

01189). Angus Calder is thanked for the X-ray diffraction data. Jason Farrell and Alan Drew are thanked for their assistance in operating the MPMS. We thank the captain and crew of the *Marion Dufresne* for their help in recovering MD95–2006 and the IMAGES program and Laurent Labeyrie, in particular, for their support. Eva Moreno and two anonymous reviewers are thanked for their helpful comments.

References

Alley, R. B., and D. R. MacAyeal (1994), Ice-rafted debris associated with binge/purge oscillations of the Laurentide Ice Sheet, *Paleoceanography*, *9*, 503–511, doi:10.1029/94PA01008.

Alley, R. B., J. T. Andrews, D. C. Barber, and P. U. Clark (2005), Comment on "Catastrophic ice shelf breakup as the source of Heinrich event icebergs" by C. L. Hulbe et al., *Paleoceanography*, *20*, PA1009, doi:10.1029/2004PA001086.

Andrews, J. T. (1998), Abrupt changes (Heinrich events) in Late Quaternary North Atlantic marine environments: A history and review of data and concepts, *J. Quat. Sci.*, *13*(1), 3–16, doi:10.1002/(SICI)1099-1417(199801/02)13:1<3::AID-JQS361>3.0.CO;2-0.

Andrews, J. T., and K. Tedesco (1992), Detrital carbonate-rich sediments, northwestern Labrador Sea: Implications for ice-sheet dynamics and iceberg rafting (Heinrich) events in the North Atlantic, *Geology*, *20*, 1087–1090, doi:10.1130/0091-7613(1992)020<1087:DCRSNL>2.3.CO;2.

Armishaw, J. E., R. W. Holmes, and D. A. V. Stow (1998), Morphology and sedimentation on the Hebrides Slope and Barra Fan, NW UK continental margin, in *Geological Processes on Continental Margins: Sedimentation, Mass-Wasting and Stability*, edited by M. S. Stoker, D. Evans, and A. Cramp, *Spec. Publ. Geol. Soc. London*, *129*, 81–104.

Austin, W. E. N., L. J. Wilson, and J. B. Hunt (2004), The age and chronostratigraphical significance of North Atlantic ash zone II, *J. Quat. Sci.*, *19*(2), 137–146, doi:10.1002/jqs.821.

Bender, M., T. Sowers, M. L. Dickson, J. Orchardo, P. M. Grootes, P. A. Mayewski, and D. A. Meese (1994), Climate correlations between Greenland and Antarctica during the past 100,000 years, *Nature*, *372*, 663–666, doi:10.1038/372663a0.

Björck, S., M. J. C. Walker, L. C. Cwynar, S. Johnsen, K.-L. Knudsen, J. J. Lowe, B. Wohlfarth, and the INTIMATE Members (1998), An event stratigraphy for the last termination in the North Atlantic region based on the Greenland ice-core record: A proposal by the INTIMATE group, *J. Quat. Sci.*, *13*(4), 283–292, doi:10.1002/(SICI)1099-1417(199807/08)13:4<283::AID-JQS386>3.0.CO;2-A.

Bond, G., et al. (1992), Evidence for massive discharges of icebergs into the North Atlantic Ocean during the last glacial period, *Nature*, *360*, 245–249, doi:10.1038/360245a0.

Bond, G., W. S. Broecker, S. Johnsen, J. McManus, L. Labeyrie, J. Jouzel, and G. Bonani (1993), Correlations between climate records from North Atlantic sediments and Greenland ice, *Nature*, *365*, 143–147, doi:10.1038/365143a0.

Bond, G., W. Showers, M. Cheseby, R. Lotti, P. Almasi, P. DeMenocal, P. Priore, H. Cullen, I. Hajdas, and G. Bonani (1997), A pervasive millennial-scale cycle in North Atlantic Holocene and glacial climates, *Science*, *278*, 1257–1266, doi:10.1126/science.278.5341.1257.

Bond, G., W. Showers, M. Elliot, M. Evans, R. Lotti, I. Hajdas, G. Bonani, and S. Johnsen (1999), The North Atlantic's 1–2 kyr climate rhythm: Relation to Heinrich events, Dansgaard/Oeschger cycles and the Little Ice Age, in *Mechanisms of Global Climate Change at Millennial Time Scales*, *Geophys. Monogr. Ser.*, vol. 112, edited by P. U. Clark, R. S. Webb, and L. D. Keigwin, pp. 35–58, AGU, Washington, D.C.

Bond, G. C., and R. Lotti (1995), Iceberg discharges into the North Atlantic on millennial time scales during the last glaciation, *Science*, *267*, 1005–1010, doi:10.1126/science.267.5200.1005.

Broecker, W. S., G. Bond, J. McManus, M. Klas, and E. Clarke (1992), Origin of the North Atlantic's Heinrich events, *Clim. Dyn.*, *6*, 265–273, doi:10.1007/BF00193540.

Carter-Stiglitz, B., B. Moskowitz, and M. Jackson (2001), Unmixing magnetic assemblages and the magnetic behaviour of bimodal mixtures, *J. Geophys. Res.*, *106*(B11), 26,397–26,411, doi:10.1029/2001JB000417.

Dansgaard, W., et al. (1993), Evidence for general instability of past climate from a 250-kyr ice-core record, *Nature*, *364*, 218–220, doi:10.1038/364218a0.

de Boer, C. B., T. A. T. Mullender, and M. J. Dekkers (2001), Low temperature behaviour of haematite: Susceptibility and magnetisation increase on cycling through the Morin transition, *Geophys. J. Int.*, *146*, 201–216, doi:10.1046/j.0956-540x.2001.01443.x.

Dekkers, M. J., J. L. Mattéi, G. Fillion, and P. Rochette (1989), Grain size dependence of the magnetic behaviour of pyrrhotite during its low temperature transition at 34 K, *Geophys. Res. Lett.*, *16*, 855–858, doi:10.1029/GL016i008p00855.

Dickson, A. J. (2004), Water mass changes and ice-sheet dynamics during marine isotope stage 3 on the northeast Atlantic continental margin, M. S. thesis, R. Holloway, Univ. of London, London.

Dowdeswell, J. A., M. A. Maslin, J. T. Andrews, and I. N. McCave (1995), Iceberg production, debris rafting, and the extent and thickness of Heinrich layers (H-1, H-2) in North Atlantic sediments, *Geology*, *23*, 301–304, doi:10.1130/0091-7613(1995)023<0297:IPDRAT>2.3.CO;2.

Dowdeswell, J. A., A. Elverhoi, J. T. Andrews, and D. Hebbeln (1999), Asynchronous deposition of ice-rafted layers in the Nordic Seas and North Atlantic Ocean, *Nature*, *400*, 348–351, doi:10.1038/22510.

Elliot, M., L. Labeyrie, and J.-C. Duplessy (2002), Changes in North Atlantic deep-water formation associated with the Dansgaard-Oeschger temperature oscillations (60–10 ka), *Quat. Sci. Rev.*, *21*, 1153–1165, doi:10.1016/S0277-3791(01)00137-8.

Farmer, G. L., D. Barber, and J. Andrews (2003), Provenance of Late Quaternary ice-proximal sediments in the North Atlantic: Nd, Sr and Pb isotopic evidence, *Earth Planet. Sci. Lett.*, *209*, 227–243, doi:10.1016/S0012-821X(03)00068-2.

Fronval, T., E. Jansen, J. Bloemendal, and S. Johnsen (1995), Oceanic evidence for coherent fluctuations in Fennoscandian and Laurentide ice sheets on millennium timescales, *Nature*, *400*, 348–351.

Grönvold, K., N. Óskarsson, S. J. Johnsen, H. B. Clausen, C. U. Hammer, G. Bond, and E. Bard (1995), Express letter: Ash layers from Iceland in the Greenland GRIP ice core correlated with oceanic and land sediments, *Earth Planet. Sci. Lett.*, *135*, 149–155, doi:10.1016/0012-821X(95)00145-3.

Grousset, F. E., L. Labeyrie, J. A. Sinko, M. Cremer, G. Bond, J. Duprat, E. Cortijo, and S. Huon (1993), Patterns of ice-rafted detritus in the glacial North Atlantic (40–55°N), *Paleoceanography*, *8*, 175–192, doi:10.1029/92PA02923.

Grousset, F. E., C. Pujol, L. Labeyrie, G. Auffret, and A. Boelaert (2000), Were the North Atlantic Heinrich events triggered by the behavior of the European ice sheets?, *Geology*, *28*, 123–126, doi:10.1130/0091-7613(2000)28<123:WTNAHE>2.0.CO;2.

Heinrich, H. (1988), Origin and consequences of cyclic ice rafting in the northeast Atlantic Ocean during the past 130,000 years, *Quat. Res.*, *29*, 142–152, doi:10.1016/0033-5894(88)90057-9.

Hemming, S. R. (2004), Heinrich events: Late Pleistocene detritus layers of the north Atlantic and their global climate imprint, *Rev. Geophys.*, *42*, RG1005, doi:10.1029/2003RG000128.

Hemming, S. R., W. S. Broecker, W. D. Sharp, G. C. Bond, R. H. Gwaizda, J. F. McManus, M. Klas, and I. Hajdas (1998), Provenance of the Heinrich layers in core V28-82, northeastern Atlantic: $^{40}Ar/^{39}Ar$ ages of ice-rafted hornblende, Pb isotopes in feldspar grains, and Nd-Sr-Pb isotopes in the fine sediment fraction, *Earth Planet. Sci. Lett.*, *164*, 317–333, doi:10.1016/S0012-821X(98)00224-6.

Hemming, S. R., T. O. Vorren, and J. Kleman (2002), Provinciality of ice rafting in the North Atlantic: Application of $^{40}Ar/^{39}Ar$ dating of individual ice rafted hornblende grains, *Quat. Int.*, *95–96*, 75–85, doi:10.1016/S1040-6182(02)00029-0.

Hillaire-Marcel, C., A.k. de Vernal, G. Bilodeau, and G. Wu (1994), Isotope stratigraphy, sedimentation rates, deep circulation, and carbonate events in the Labrador Sea during the last ~200 ka, *Can. J. Earth Sci.*, *31*, 68–89.

Holmes, R., D. Long, and L. R. Dodd (1998), Large-scale debrites and submarine landslides on the Barra Fan, west of Britain, in *Geological Processes on Continental Margins: Sedimentation, Mass-Wasting and Stability*, edited by M. S. Stoker, D. Evans, and A. Cramp, *Spec. Publ. Geol. Soc. London*, *129*, 67–79.

Johnsen, S. J., H. B. Clausen, W. Dansgaard, K. Fuhrer, N. Gundestrump, C. U. Hammer, P. Iversen, J. Jouzel, B. Stauffer, and J. P. Steffensen (1992), Irregular glacial interstadials recorded in a new Greenland ice core, *Nature*, *359*, 311–313, doi:10.1038/359311a0.

Johnsen, S. J., D. Dahl-Jensen, N. Gundestrup, J. P. Steffensen, H. B. Clausen, H. Miller, V. Masson-Delmotte, A. E. Sveinbjörnsdottir, and J. White (2001), Oxygen isotope and palaeotemperature records from six Greenland ice-core stations: Camp Century, Dye-3, GRIP, GISP2, Renland and NorthGRIP, *J. Quat. Sci.*, *16*(4), 299–307, doi:10.1002/jqs.622.

King, J., S. K. Banerjee, J. Marvin, and Ö. Özdemir (1982), A comparison of different magnetic methods for determining the relative grain size of magnetite in natural materials: Some results from lake sediments, *Earth Planet. Sci. Lett.*, *59*, 404–419, doi:10.1016/0012-821X(82)90142-X.

Kissel, C. (2005), Magnetic signature of rapid climatic variations in glacial North Atlantic, a review, *C. R. Geosci.*, *337*, 908–918, doi:10.1016/j.crte.2005.04.009.

Knutz, P. C., W. E. N. Austin, and E. J. W. Jones (2001), Millennial-scale depositional cycles related to British ice sheet variability and North Atlantic paleocirculation since 45 kyr B. P., Barra Fan, U.K. margin, *Paleoceanography*, *16*, 53–64, doi:10.1029/1999PA000483.

Kroon, D., G. Shimmield, W. E. N. Austin, S. Derrick, P. Knutz, and T. Shimmield (2000), Century- to millennial-scale sedimentological-

geochemical records of glacial-Holocene sediment variations from the Barra Fan (NE Atlantic), *J. Geol. Soc. London*, *157*, 643–653.

Leigh, S. N. B. (2006), A study of the dynamics of the British ice sheet during Marine Isotope Stages 2 and 3 focusing on Heinrich Events 2 and 4 and their relationship to the North Atlantic glaciological and climatological conditions, M. S. thesis, Univ. of St. Andrews, St. Andrews, U.K.

Liu, Q., S. K. Banerjee, M. J. Jackson, R. Zhu, and Y. Pan (2002), A new method in mineral magnetism for the separation of weak antiferromagnetic signal from a strong ferrimagnetic background, *Geophys. Res. Lett.*, *29*(12), 1565, doi:10.1029/2002GL014699.

MacAyeal, D. R. (1993), Binge/purge oscillations of the Laurentide ice sheet as a cause of the North Atlantic's Heinrich events, *Paleoceanography*, *8*, 775–784, doi:10.1029/93PA02200.

Martinson, D. G., N. G. Pisias, J. D. Hays, J. Imbrie, T. C. Moore Jr., and N. J. Shackleton (1987), Age dating and the orbital theory of the ice ages: Development of a high-resolution 0 to 300,000-year chronostratigraphy, *Quat. Res.*, *27*, 1–29, doi:10.1016/0033-5894(87)90046-9.

McManus, J. F., G. C. Bond, W. S. Broecker, S. Johnsen, L. Labeyrie, and S. Higgins (1994), High-resolution climate records from the North Atlantic during the last interglacial, *Nature*, *371*, 326–329, doi:10.1038/371326a0.

Meese, D. A., et al. (1994), Preliminary depth-age scale of the GISP2 ice core, *Spec. Rep. 94-1*, Cold Reg. Res. and Eng. Lab., Hanover, N.H.

Moreno, E., N. Thouveny, D. Delanghe, I. N. McCave, and N. J. Shackleton (2002), Climatic and oceanographic changes in the Northeast Atlantic reflected by magnetic properties of sediments deposited on the Portuguese Margin during the last 340 ka, Earth Planet, *Sci. Lett.*, *202*, 465–480, doi:10.1016/S0012-821X(02)00787-2.

Morin, J. (1950), Magnetic susceptibility of α-Fe_2O_3 and Fe_2O_3 with added titanium, *Phys. Rev.*, *78*, 819–820, doi:10.1103/PhysRev.78.819.2.

Moros, M., A. Kuijpers, I. Snowball, S. Lassen, D. Bäckström, F. Gingele, and J. McManus (2002), Were glacial iceberg surges in the North Atlantic triggered by climate warming?, *Mar. Geol.*, *192*, 393–417, doi:10.1016/S0025-3227(02)00592-3.

Moros, M., J. F. McManus, T. Rasmussen, A. Kuijpers, T. Dokken, I. Snowball, T. Nielsen, and E. Jansen (2004), Quartz content and the quartz-to-plagioclase ratio determined by X-ray diffraction: A proxy for ice rafting in the northern North Atlantic?, *Earth Planet. Sci. Lett.*, *218*, 389–401, doi:10.1016/S0012-821X(03)00675-7.

Moskowitz, B. M., M. Jackson, and C. Kissel (1998), Low-temperature magnetic behavior of titanomagnetites, *Earth Planet. Sci. Lett.*, *157*, 141–149, doi:10.1016/S0012-821X(98)00033-8.

North Greenland Ice Core Project Members (2004), High-resolution record of Northern Hemisphere climate extending into the last interglacial period, *Nature*, *431*, 147–151, doi:10.1038/nature02805.

O'Reilly, W. (1984), *Rock and Mineral Magnetism*, Blackie Acad. and Prof., Glasgow, U.K.

Özdemir, Ö., D. J. Dunlop, and B. M. Moskowitz (1993), The effect of oxidation on the Verwey transition in magnetite, *Geophys. Res. Lett.*, *20*, 1671–1674, doi:10.1029/93GL01483.

Peters, C. (1995), Unravelling magnetic mixtures in sediments, soils and rocks, Ph.D. thesis, Univ. of Edinburgh, Edinburgh, U.K.

Peters, C., and M. J. Dekkers (2003), Selected room temperature magnetic parameters as a function of mineralogy, concentration and grain size, *Phys. Chem. Earth*, *28*, 659–667.

Peters, C., and G. Turner (1999), Lake Paringa: A catchment study using magnetic techniques, *Phys. Chem. Earth*, *24*, 753–757, doi:10.1016/S1464-1895(99)00110-6.

Pflaumann, U., et al. (2003), Glacial North Atlantic: Sea-surface conditions reconstructed by GLAMAP 2000, *Paleoceanography*, *18*(3), 1065, doi:10.1029/2002PA000774.

Rahmstorf, S. (1996), On the freshwater forcing and transport of the Atlantic thermohaline circulation, *Clim. Dyn.*, *12*, 799–811, doi:10.1007/s003820050144.

Rashid, H., R. Hesse, and D. J. W. Piper (2003), Evidence for an additional Heinrich event between H5 and H6 in the Labrador Sea, *Paleoceanography*, *18*(4), 1077, doi:10.1029/2003PA000913.

Richter, T. O., S. Lassen, T. C. E. van Weering, and H. de Haas (2001), Magnetic susceptibility patterns and provenance of ice-rafted material at Feni Drift, Rockall Trough: Implications for the history of the British-Irish ice sheet, *Mar. Geol.*, *173*, 37–54, doi:10.1016/S0025-3227(00)00165-1.

Robinson, S. G., M. A. Maslin, and I. N. McCave (1995), Magnetic susceptibility variations in Late Pleistocene deep-sea sediments of the northeast Atlantic: Implications for ice rafting and paleocirculation at the last glacial maximum, *Paleoceanography*, *10*, 221–250, doi:10.1029/94PA02683.

Rousseau, D. D., G. Kukla, and J. McManus (2006), What is what in the ice and the ocean?, *Quat. Sci. Rev.*, *25*, 2025–2030, doi:10.1016/j.quascirev.2006.03.009.

Ruddiman, W. F. (1977), Late Quaternary deposition of ice-rafted sand in the subpolar North Atlantic (lat 40° to 65°N), *Geol. Soc. Am. Bull.*, *88*, 1813–1827, doi:10.1130/0016-7606(1977)88<1813:LQDOIS>2.0.CO;2.

Sagnotti, L., P. Rochette, M. Jackson, F. Vadeboin, J. Dinarès-Turell, A. Winkler, and "Magnet" Science Team (2003), Inter-laboratory calibration of low-field magnetic and anhysteretic susceptibility measurements, *Phys. Earth Planet. Inter.*, *138*, 25–38, doi:10.1016/S0031-9201(03)00063-3.

Scourse, J. D., I. R. Hall, I. N. McCave, J. R. Young, and C. Sugdon (2000), The origin of Heinrich layers: Evidence from H2 for European precursor events, *Earth Planet. Sci. Lett.*, *182*, 187–195, doi:10.1016/S0012-821X(00)00241-7.

Shankar, R., R. Thompson, and R. B. Galloway (1994), Sediment source modelling: Unmixing of artificial magnetisation and natural radioactivity measurements, *Earth Planet. Sci. Lett.*, *126*, 411–420, doi:10.1016/0012-821X(94)90121-X.

Snoeckx, H., F. E. Grousset, M. Revel, and A. Boelaert (1999), European contribution of ice-rafted sand to Heinrich layers H3 and H4, *Mar. Geol.*, *158*, 197–208, doi:10.1016/S0025-3227(98)00168-6.

Stoner, J. S., J. E. Channell, and C. Hillaire-Marcel (1996), The magnetic signature of rapidly deposited detrital layers from the deep Labrador Sea: Relationship to North Atlantic Heinrich layers, *Paleoceanography*, *11*, 309–325, doi:10.1029/96PA00583.

Thompson, R. (1986), Modelling magnetization data using SIMPLEX, *Phys. Earth Planet. Inter.*, *42*, 113–127, doi:10.1016/S0031-9201(86)80013-9.

Verwey, E. J. W., and P. W. Haayman (1941), Electronic conductivity and transition point in magnetite, *Physics*, *8*, 979–982.

Walden, J., M. C. Slattery, and T. P. Burt (1997), Use of mineral magnetic measurements to fingerprint suspended sediment sources: Approaches and techniques for data analysis, *J. Hydrol.*, *202*, 353–372, doi:10.1016/S0022-1694(97)00078-4.

Walden, J., E. R. Wadsworth, W. E. N. Austin, C. Peters, J. D. Scourse, and I. R. Hall (2007), Compositional variability of ice-rafted debris in Heinrich layers 1 and 2 on the northwest European continental slope identified by environmental magnetic analyses, *J. Quat. Sci.*, *22*(2), 163–172, doi:10.1002/jqs.1020.

Walden, J., C. Peters, W. E. N. Austin, I. L. Millar, and E. Wadsworth (2008), Modelling changes in ice-rafted debris sources through Heinrich Event 2 and Heinrich Event 1 on the NE European continental slope using environmental magnetic, radiogenic isotope and X-ray diffraction analysis of marine sediments, *Geophys. Res. Abstr.*, *10*, EGU2008-A-06727.

Walker, M. J. C., S. Björck, J. J. Lowe, L. C. Cwynar, S. Johnsen, K-L. Knudsen, B. Wohlfarth, and INTIMATE Group (1999), Isotopic 'events' in the GRIP ice core: A stratotype for the Late Pleistocene, *Quat. Sci. Rev.*, *18*, 1143–1150, doi:10.1016/S0277-3791(98)00119-X.

Watkins, S. J. (2003), Geological ground-truthing of modelled iceberg trajectories in the North Atlantic: Present day and the last glacial maximum, Ph.D. thesis, Univ. of East Anglia, Norwich, U.K.

Wilson, L. J., and W. E. N. Austin (2002), Millennial and sub-millennial-scale variability in sediment colour from the Barra Fan, N. W. Scotland: Implications for British ice sheet dynamics, in *Glacier-Influenced Sedimentation on High-Latitude Continental Margins*, edited by J. A. Dowdeswell and C. Ó. Cofaigh, *Spec. Publ. Geol. Soc. London*, *203*, 349–365.

Wilson, L. J., W. E. N. Austin, and E. Jansen (2002), The last British ice sheet: Growth, maximum extent and deglaciation, *Polar Res.*, *21*, 243–250, doi:10.1111/j.1751-8369.2002.tb00077.x.

Yu, L., and F. Oldfield (1989), A multivariate mixing model for identifying sediment source from magnetic measurements, *Quat. Res.*, *32*, 168–181, doi:10.1016/0033-5894(89)90073-2.

Zaragosi, S., F. Eynaud, C. Pujol, G. A. Auffret, J.-L. Turon, and T. Garlan (2001), Initiation of European deglaciation as recorded in the northwestern Bay of Biscay slope environments (Meriadzek Terrace and Trevelyan Escarpment): A multi-proxy approach, *Earth Planet. Sci. Lett.*, *188*, 493–507, doi:10.1016/S0012-821X(01)00332-6.

Zielinski, G. A., P. A. Mayewski, L. D. Meeker, K. Grönvold, M. S. Germani, S. Whitlow, M. S. Twickler, and K. Taylor (1997), Volcanic aerosol records and tephrochronology of the Summit, Greenland, ice cores, *J. Geophys. Res.*, *102*(C12), 26,625–26,640, doi:10.1029/96JC03547.

W. E. N. Austin, C. Peters, and J. Walden, Environmental Change Research Group, School of Geography and Geosciences, University of St. Andrews, St. Andrews KY16 9AL, UK. (cp34@st-andrews.ac.uk)